Review of Scientific Instruments

Robust finite-time adaptive control for high performance voice coil motor-actuated fast steering mirror

Cite as: Rev. Sci. Instrum. **93**, 125003 (2022); https://doi.org/10.1063/5.0124203
Submitted: 04 September 2022 • Accepted: 11 November 2022 • Published Online: 02 December 2022

Lina Wang, Zhongshi Wang, Fuchao Wang, et al.

AIP Publishing

Review of Scientific Instruments ARTICLE scitation.org/journal/rsi

Robust finite-time adaptive control for high performance voice coil motor-actuated fast steering mirror

Cite as: Rev. Sci. Instrum. 93, 125003 (2022); doi: 10.1063/5.0124203
Submitted: 4 September 2022 • Accepted: 11 November 2022 •
Published Online: 2 December 2022

Lina Wang,[1] Zhongshi Wang,[2] Fuchao Wang,[2] Guangfeng Shi,[1] and Rui Xu[2,a)]

AFFILIATIONS

[1] College of Electro-Mechanical Engineering, Changchun University of Science and Technology, Changchun 130022, China
[2] Key Laboratory of Airborne Optical Imaging and Measurement, Changchun Institute of Optics, Fine Mechanics and Physics, Chinese Academy of Sciences, Changchun 130033, China

[a)] **Author to whom correspondence should be addressed:** xur@ciomp.ac.cn

ABSTRACT

Fast steering mirror (FSM) is an efficient and reliable mechanical device in aerial optical image systems for controlling the beam direction with high precision. With the advantages of compact size, high speed, simple structure, and long linear stroke, voice coil motors are ideal actuators for FSM systems. However, model uncertainty can lead to poor performance or even system divergence, especially in environments with temperature variations, electromagnetic environment changes, etc. This paper proposes a novel finite-time adaptive control (FAC) algorithm for an FSM system to obtain high performance, i.e., positioning accuracy, dynamic performance, and robustness. In addition, the finite-time convergence of the controller is analyzed. In the experiments, the controller is implemented in a DSP-based microprocessor. The step response results show that the proposed algorithm has a shorter setting time, smaller overshoot, and smaller steady-state error compared to classical sliding mode control (SMC). The sinusoidal signal tracking accuracy of FAC + SMC has been improved by 19.8%. In addition, as the model uncertainty increases 10%, the root mean square errors (RMSEs) are 1.73″ and 1.18″ for SMC and FAC + SMC, respectively. With 20% model uncertainty, the RMSEs increase to 2.56″ and 1.85″, respectively. Extensive experiments demonstrate the general effectiveness of the proposed algorithm.

NOMENCLATURE

τ_a	The output torque of the system
K_a	The equivalent torque coefficient
i_a	The total current in the system
u	The control voltage of the system
R_a	The equivalent resistance
L_a	The equivalent inductance
e_a	The back electromotive force
K_e	The back electromotive force coefficient
$\theta, \dot{\theta}, \ddot{\theta}$	The angle, angular velocity, and angular acceleration of the FSM
J_m, B_m, K_m	The equivalent moment of inertia, viscous damping, and stiffness parameters
p_0, p_1, p_2	The parameters of the general FSM model
d	The model uncertainty and the external disturbance
σ	The sliding mode surface
c_1, c_2	The positive parameters determine the state error's converging speed when the system is on the sliding mode surface
θ_d	The desired angle
$e, \dot{e}, \ddot{e}$	The angular error, angular velocity error, and angular acceleration error
k_s	The switching-gain of the SMC
k_a	The adaptive control value
$sign(\cdot)$	The switching function
k_1, k_2, k_3	The positive parameters of the adaptive control law
T	The setting time.
V	The Lyapunov function

I. INTRODUCTION

Aerial optical imaging systems, such as infrared search systems,[1] laser pointing systems,[2] tracking and targeting systems,[3] and

observation systems,[4] all require high-performance actuators to isolate the movement of the aircraft and various disturbances to achieve stable imaging. There are two general approaches: platform stabilization and steering stabilization.[5] However, limited by the large inertia and the complexity of disturbance, it is difficult to improve the stability accuracy of line-of-sight (LOS) by relying on platform stabilization.

In the second approach, the direction of the LOS is controlled by rotating a movable optical element, i.e., fast steering mirror (FSM), in the optical path.[6] The FSM is a high-precision manufacturing device involving mechanical structures, controllers, and measurement sensors for precise control of the beam direction.[7] It has advantages of low inertia, high stiffness, and large energy density and is widely used in various optical imaging systems. Although the current commercially available FSMs can provide satisfactory performance in certain scenarios when advanced aerospace equipment performs long-distance communication/tracking missions, a high level of stabilization accuracy is required from the FSM. Thus, the original motivation of this study is to improve the positioning accuracy of FSMs.

Depending on the actuator, FSMs can be classified as voice coil motor (VCM)-actuated and piezoelectric-actuated FSMs. The piezoelectric actuators are based on the inverse piezoelectric effect to achieve motion. Due to their high positioning accuracy, many researchers have investigated piezoelectric-actuated FSMs guided by a ring-type flexible hinge and high-bandwidth high-precision tracking control methods.[8] The piezoelectric-actuated FSMs can achieve a relatively high positioning accuracy but suffer from the problem of short-stroke.[9] Furthermore, according to the author's previous research, hysteresis nonlinearity, which is a complex behavior with amplitude-dependent, rate-dependent, and temperature-dependent,[10] may lead to complex controller designs and is, therefore, difficult to apply in practical engineering.

The VCM is a current-driven linear motor, consisting mainly of a moving coil and a permanent magnet. It has the advantages of compact size, high speed, simple structure, and long linear stroke. Due to these advantages, VCMs have been used in many precision motion applications.[11] For instance, Al-Jodah *et al.* developed a large-range 1-degree-of-freedom stage based on the VCM. The sliding mode control (SMC) is augmented with an adaptive fuzzy disturbance observer, which achieves the high precision of tracking performance.[12] A Lorentz force fast tool servo is designed in which the VCM is located inside the slide, and a novel advanced proportional-integral-differential (PID) control with velocity/acceleration feed-forward and SMC is implemented with the tracking error subsequently decreasing to 0.871% at 50 Hz.[13] Wang *et al.* proposed the direct amplitude control to maintain the amplitude of a VCM-based high-frequency reciprocating rig under frictional loads.[14]

Recently, many researchers have worked on high-precision VCM-actuated FSM systems.[15] There are two important research directions: one is to improving the anti-disturbance ability and the other is to improving the command tracking accuracy. Therefore, the control methods of VCM-actuated FSMs are mainly based on the composite control of feed-forward control and anti-disturbance control. For example, an active disturbance rejection control algorithm is used in the controller design of the FSM, which eliminates system disturbances and improves speed accuracy.[16] A model reference adaptive controller is proposed to further improve the control accuracy of the FSM to eliminate the dependence on the accuracy of the system model.[17] A control algorithm based on the disturbance observer and H∞ is proposed, which improves the current dynamic characteristic and robustness of the VCM.[18] An improved repetitive control of the tip–tilt mirror is proposed, which can reduce telescope vibrations and achieve optimal performance when vibrations are provided.[19] These studies are premised on obtaining accurate model parameters. However, model uncertainty persists in many cases, which may lead to poor performance or even system divergence. In particular, in some special applications, such as temperature variations and electromagnetic environment changes, the characteristics of the system change greatly, resulting in a large increase in the model uncertainty.

The primary consideration in the controller design is stability. In contrast to classical Lyapunov stability, finite-time stability ensures that the system states converge quickly to the equilibrium point in finite time.[20,21] The finite-time control has achieved good results.[22,23] For instance, the adaptive finite-time and fixed-time control schemes of the permanent magnet synchronous motor (PMSM) in a noise environment are proposed, which not only ensure fast stochastic chaos synchronization of PMSMs but also successfully determine the control gain.[24] A non-singular fast terminal sliding mode and finite-time disturbance observer techniques are deployed in a surface vehicle; experimental results show that the trajectory tracking error can reach exactly zero in finite time.[25] However, to the best of the author's knowledge, there has been little research on finite-time control and adaptive SMC in the field of VCM-actuated FSM. Therefore, this paper considers exploiting the excellent robustness of adaptive control and the fast convergence of finite-time control.

In summary, to improve the robustness to model uncertainty and to speed up the convergence of the control error, a robust finite-time adaptive controller (FAC) is proposed in this paper that combines finite-time control with adaptive SMC. Compared with the state of the art, the main innovations are as follows:

(1) A control algorithm is proposed for VCM-actuated FSM systems, which is robust to model uncertainty. A novel adaptive law is proposed in the FAC to obtain finite-time convergence behavior.
(2) The controller is simple in form, with an adaptive control value added to the classical sliding mode controller. As a result, it is easy to implement. The parameters have a clear mathematical meaning and are easy to tune.

The rest of this paper is organized as follows. First, in Sec. II, the VCM-driven FSM mechanics are presented and a general mathematical model is developed. Then, in Sec. III, the controller design of the VCM-actuated FSM is presented and finite-time stability is analyzed. Section IV describes comparative experiments of the controller to measure the performance of the proposed FAC. Finally, conclusions are presented in Sec. V.

II. MODELING AND ANALYSIS

The FSM system is based on a push–pull pattern of two VCMs and a flexible hinge to achieve rotation. The principle of motion is shown in Fig. 1.

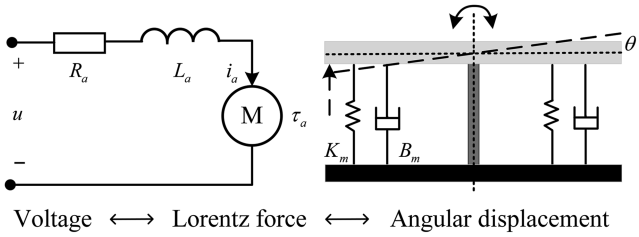

FIG. 1. Schematic diagram of the FSM movement principle.

With a constant number of coil turns and magnetic field strength, the Lorentz force of VCMs is closely proportional to the current. In the push–pull mode, the two VCMs are placed symmetrically so that the output torque is proportional to the current of the FSM system,

$$\tau_a(t) = K_a i_a(t), \tag{1}$$

where $\tau_a(t)$ is the output torque of the system, K_a is the equivalent torque coefficient, and $i_a(t)$ is the total current in the system.

Then, according to the voltage balance equation, the total current of the system can be obtained,

$$u(t) - e_a(t) = R_a i_a(t) + L_a \dot{i}_a(t), \tag{2}$$

where $u(t)$ is the control voltage of the system, R_a and L_a are the equivalent resistance and inductance, respectively, and $e_a(t)$ is the back electromotive force, which is related to the angular velocity of rotation of the FSM,

$$e_a(t) = K_e \dot{\theta}(t), \tag{3}$$

where K_e is the back electromotive force coefficient, $\theta(t)$ is the angle of the FSM, and $\dot{\theta}(t)$ represents the angular velocity.

According to rigid body dynamics, the rotational motion of the FSM can be described as follows:

$$\tau_a(t) = J_m \ddot{\theta}(t) + B_m \dot{\theta}(t) + K_m \theta(t), \tag{4}$$

where J_m, B_m, and K_m are the equivalent moment of inertia, viscous damping, and stiffness constant parameters, respectively.

Since the inductance is usually small, it can be neglected, i.e., $L_a \approx 0$. Arranging Eqs. (1)–(4) yields the following results:

$$J_m \ddot{\theta}(t) + \left(B_m + \frac{K_a K_e}{R_a}\right)\dot{\theta}(t) + K_m \theta(t) = \frac{K_a}{R_a} u(t). \tag{5}$$

A general description of the FSM model is given,

$$\ddot{\theta}(t) = p_0 \dot{\theta}(t) + p_1 \theta(t) + p_2 u(t), \tag{6}$$

where the parameters of the model are defined, i.e., $p_0 = -\frac{(R_a B_m + K_a K_e)}{J_m R_a}$, $p_1 = -\frac{K_m}{J_m}$, and $p_2 = \frac{K_a}{J_m R_a}$. Considering the equivalent disturbance, the general model (6) can be described as follows:

$$\ddot{\theta}(t) = p_0 \dot{\theta}(t) + p_1 \theta(t) + p_2 (u(t) + d(t)), \tag{7}$$

where $d(t)$ contains the model uncertainty and the external disturbance.

III. CONTROLLER DESIGN

In this section, we will investigate the controller design method with model uncertainty compensation.

A. Preliminaries

Before implementing the controller design, some results on finite-time stability are reviewed.

Definition 1 (see Ref. 26). For a differential-equation-based system,

$$\dot{x}(t) = f(x(t)), x \in \mathbb{R}, \tag{8}$$

with a continuous function $f(\cdot)$ such that $f(0) = 0$, the system is globally finite-time stable if it is Lyapunov stable, and for all $x_0 \in \mathbb{R}$, there exists $T(x_0) \geq 0$ dependent on the initial conditions such that for any $x(\cdot)$ solution of the differential equation with $x(0) = x_0$, $lim_{t \to T(x_0)} \|x(t)\| = 0$, i.e., $\|x(t)\| \equiv 0$ for all $t \geq T(x_0)$. The function T is called the setting time.

Lemma 1 (see Ref. 24). If $z_1, z_2, \ldots, z_n \geq 0$, then

$$\sum_{i=1}^{n} z_i^v \geq \left(\sum_{i=1}^{n} z_i\right)^v, \quad 0 < v \leq 1, \tag{9}$$

in which "=" holds for $v = 1$.

Lemma 2 (see Ref. 27). For a system (8), if there exists a continuous positive definite function V such that

$$\dot{V}(x) \leq -\lambda V^{\mu}(x)), \quad \forall x \in \mathbb{D}n\{0\}, \tag{10}$$

where $\lambda > 0$ and $0 < \mu < 1$, the origin of the system is globally finite-time stable and the setting time satisfies

$$T \leq \frac{V^{1-\mu}(x_0)}{\lambda(1-\mu)}, \quad x_0 \in \mathbb{U}. \tag{11}$$

Lemma 3 (see Ref. 28). For a system (8), if there exists a continuous positive definite function V such that

$$\dot{V}(x) \leq -\lambda V^{\mu}(x) + \eta V(x), \quad \forall x \in \mathbb{D}\backslash\{0\}, \tag{12}$$

where $\lambda, \eta > 0$ and $0 < \mu < 1$, then the origin of system (8) is semi-global finite-time stable. The set

$$\mathbb{U} = \{x | V^{1-\mu}(x) < \frac{\lambda}{\eta}\} \cap \mathbb{D} \tag{13}$$

is contained in the domain of attraction of the origin. The setting time satisfies

$$T \leq \frac{\ln\left(1 - \frac{\eta}{\lambda} V^{1-\mu}(x_0)\right)}{\eta(1-\mu)}, \quad x_0 \in \mathbb{U}. \tag{14}$$

B. Robust finite-time adaptive controller

To achieve robust finite-time adaptive control of the VCM-actuated FSM, we first employ the SMC and define the surface as follows:

$$\sigma(t) = c_1 e(t) + c_2 \int_0^t e(\tau)d\tau + \dot{e}(t), \tag{15}$$

where $\sigma(t)$ is the sliding mode surface and c_1 and c_2 are positive parameters determining the converging speed of the state error when the system is on the surface. The angular error is defined as

$$e(t) = \theta_d(t) - \theta(t), \tag{16}$$

where $\theta_d(t)$ and $\theta(t)$ denote the desired and actual angle, respectively. Thus, the first- and second-order derivatives, i.e., the angular velocity error and the angular acceleration error, are defined as follows:

$$\dot{e}(t) = \dot{\theta}_d(t) - \dot{\theta}(t), \quad \ddot{e}(t) = \ddot{\theta}_d(t) - \ddot{\theta}(t). \tag{17}$$

Traditional SMCs often encounter chattering problems caused by high switching gain. To reduce this effect, we consider adding an adaptive term to the existing SMC, which increases the control value when the model uncertainty increases and returns to SMC when the model uncertainty is small. In addition, to speed up the convergence process, the controller implementation must satisfy the finite-time convergence property. The proposed controller is designed as follows:

$$u(t) = \frac{1}{p_2}\ddot{\theta}_d(t) + \frac{c_1}{p_2}\dot{\theta}_d(t) + \frac{c_2}{p_2}\theta_d(t) - \frac{c_1 + p_0}{p_2}\dot{\theta}(t) - \frac{c_2 + p_1}{p_2}\theta(t) + k_s\,\mathrm{sign}(\sigma(t)) + k_a(t), \tag{18}$$

where k_s is the switching-gain of the SMC, $k_a(t)$ is the adaptive control value, and the function $\mathrm{sign}(\cdot)$ is the switching function.

From (18), it can be found that the controller contains the feedforward control value, the state feedback control value, the switching control value, and the adaptive control value. The proposed adaptive control law is as follows:

$$\dot{k}_a(t) = -k_1 k_a(t) + k_2\sigma(t) - k_3 sign(k_a(t)), \tag{19}$$

where the parameters satisfy $k_1 > 0, k_2 > 0, k_3 > 0$.

Theorem 1. *For model (7) and controller (18), with $\theta(t) \in \mathbb{R}$, the model uncertainty $d(t) \in \mathbb{R}$ has a upper bound $|d(t)| < \delta$. For given these $k_s > \delta > 0, k_1 > 0, k_2 > 0, k_3 > 0$, the closed-loop system is finite-time stable with the setting time T satisfying*

$$T \le \frac{2\ln\left(1 - \frac{|k_2-1|}{\sqrt{2}\min\{k_s-\delta,k_3\}}V^{\frac{1}{2}}(x_0)\right)}{|k_2-1|}. \tag{20}$$

Proof 1. To simplify the proof, the time-varying notation "(t)" is omitted in the following. First, a positive definite Lyapunov function is chosen,

$$V = \frac{1}{2}\sigma^2 + \frac{1}{2}k_a^2. \tag{21}$$

The time derivative of V is

$$\dot{V} = \dot{\sigma}\sigma + \dot{k}_a k_a. \tag{22}$$

Taking the time derivative of the sliding mode surface and the adaptive control law into Eq. (22) yields

$$\begin{aligned}\dot{V} &= (d - k_s\,\mathrm{sign}(\sigma) - k_a)\sigma + (k_2\sigma - k_1 k_a - k_3 sign(k_a))k_a \\ &= d\sigma - k_s|\sigma| - k_a\sigma - k_1 k_a^2 + k_2 k_a\sigma - k_3|k_a| \\ &\le (\delta - k_s)|\sigma| - k_3|k_a| + (k_2 - 1)k_a\sigma \\ &\le -\min\{k_s - \delta, k_3\}(|\sigma| + |k_a|) + (k_2 - 1)k_a\sigma.\end{aligned} \tag{23}$$

According to the inequality $k_a\sigma \le \frac{k_a^2+\sigma^2}{2}$, the equation can be written as follows:

$$\dot{V} \le -\min\{k_s - \delta, k_3\}(|\sigma| + |k_a|) + |k_2 - 1|\frac{k_a^2 + \sigma^2}{2}. \tag{24}$$

In light of Lemma 1, in which the inequality for $v = \frac{1}{2}$ is used, we get

$$\dot{V} \le -\sqrt{2}\min\{k_s - \delta, k_3\}V^{\frac{1}{2}} + |k_2 - 1|V. \tag{25}$$

Based on Lemma 3, the setting time is

$$T \le \frac{2\ln\left(1 - \frac{|k_2-1|}{\sqrt{2}\min\{k_s-\delta,k_3\}}V^{\frac{1}{2}}(x_0)\right)}{|k_2-1|}. \tag{26}$$

Remark 1. The parameters p_0, p_1, p_2 in controller (18) are derived from the model, which can be obtained by offline or online model identification methods. The parameters c_1, c_2, k_s come from the traditional SMC, and the parameter tuning method is relatively mature.

Remark 2. The desired angle signal $\boldsymbol{\theta}_d(t)$, the angular velocity signal $\dot{\boldsymbol{\theta}}_d(t)$, and the angular acceleration signal $\ddot{\boldsymbol{\theta}}_d(t)$ are required by the controller. In engineering applications, the desired signal is usually predefined so that the angular velocity and the angular acceleration signals can be obtained easily. The variable $\boldsymbol{\theta}(t)$ usually is obtained by the angle or displacement sensor, and $\dot{\boldsymbol{\theta}}(t)$ can be obtained by the differential tracker method.

Remark 3. The most important part of the method proposed is the adaptive control value $k_a(t)$, which is determined by the parameters k_1, k_2, k_3. According to (19), $k_a(t)$ is exponentially convergent to the neighborhood of $\boldsymbol{\sigma}(t)$, i.e., $\boldsymbol{\sigma}(t) \pm \frac{k_3}{k_2}$, and the convergence speed is determined by k_1. When the system is far away from the sliding mode surface $|\boldsymbol{\sigma}| \gg 0$, k_a takes a large value with $\boldsymbol{\sigma}$ so that a large approach speed can be obtained. When the system is close to the sliding mode surface, k_a obtains a small value with $\boldsymbol{\sigma}$*, which can adaptively adjust the control value to offset the changes of the model uncertainty. Because of this, the switching gain of SMC does not have to be chosen too high and the chatting of the system is reduced.*

Remark 4. Note that when $k_2 = 1$, inequality (25) can be rewritten as follows:

$$\dot{V} \le -\sqrt{2}\min\{k_s - \delta, k_3\} V^{\frac{1}{2}}. \tag{27}$$

According to Lemma 2, the system is globally finite-time stable, and the setting time satisfies

$$T \le \frac{2V^{\frac{1}{2}}(x_0)}{\sqrt{2}\min\{k_s - \delta, k_3\}}. \tag{28}$$

IV. EXPERIMENTS

A. Experimental setup

An overview of the experimental setup is represented in Fig. 2. To evaluate the proposed method, a VCM-actuated FSM system based on a flexible hinge is developed. The mirror size is 35×43 mm^2, and the steering angle of the FSM system is $\pm 1^\circ$. The first-order resonant frequency of the system is 30 Hz, and the damping ratio is 0.45.

A regulated power supply provides 24 V to the DCDC module, which outputs ±15 and 5 V to the FSM system. The proposed controller is implemented in a DSP-based circuit containing a high-performance microcontroller and a high-power amplifier.

The rotation angle of the FSM is calculated from the data sensed by the eddy current sensor. The two probes of the eddy current sensor are placed symmetrically on either side of the flexible hinge, and it measures the distance between the probe and the metal based on the eddy current effect and then calculates the steering angle of the mirror. The signal from the sensors is then picked up by using a homemade readout circuit. The sample time of the control system is set to 0.2 ms.

B. Parameters setting

The primary task of the experiment is to identify the model parameters of the controlled object, i.e., p_0, p_1, p_2 in Eq. (7). The parameters of the FSM system are obtained offline by the noise sweep method. Specifically, a small-amplitude random noise signal is used as the input signal to the system, and at the same time, the steering angle obtained by the eddy current sensor is collected. The input and output data are transferred from the DSP to the PC via the RS422toUSB cable. The data are processed according to spectral analysis methods, and then, the transfer function can be calculated. The transfer function is approximated by the least squares method. The measured and fitted open-loop Bode curves of the FSM system are demonstrated in Fig. 3.

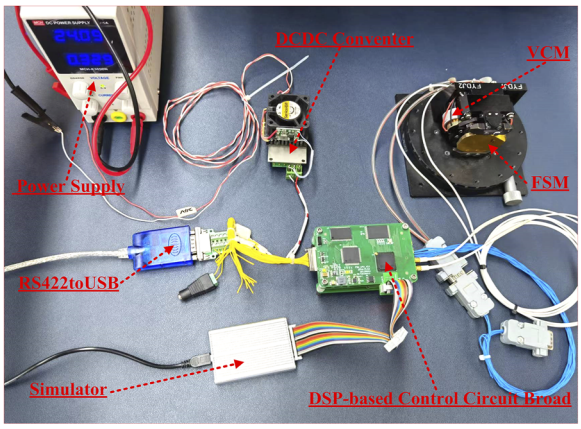

FIG. 2. Overview of the experimental setup.

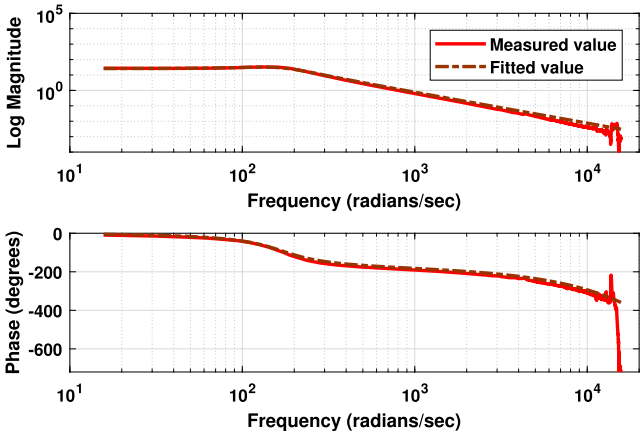

FIG. 3. Measured and fitted open-loop Bode curves.

The parameters are calculated by using the least squares method, $p_0 = -153, p_1 = -28\,900, p_2 = 751\,400$. To verify the effectiveness of the proposed algorithm, the classical SMC is selected for comparison in the experiments. Three different inputs are used in the experiments: step response, sinusoidal response, and robustness to model uncertainty.

In all experiments, the switching function is replaced by a saturation function to reduce the chattering effect, and the threshold is set as $\Delta = 200$. The other parameters in the experiment are fine-tuned. For comparison, the same parameters of the SMC are used, that is, to verify the effect of adding the FAC to the SMC. All the parameters are listed in Table I.

C. Step signal tracking performance

A 360″ step signal is used as an input to excite the FSM system. For a comprehensive analysis of the algorithm, the input signal, response signal, angle error, sliding surface, control value, and adaptive law are given in Fig. 4. The performance metrics of the step response are listed in Table II.

TABLE I. Parameters setting of the FSM system.

Method	Parameters
SMC	$c_1 = 1400, c_2 = 90\,000.$
FAC + SMC	$c_1 = 1400, c_2 = 90\,000,$ $k_1 = 9000, k_2 = 1, k_3 = 0.01.$

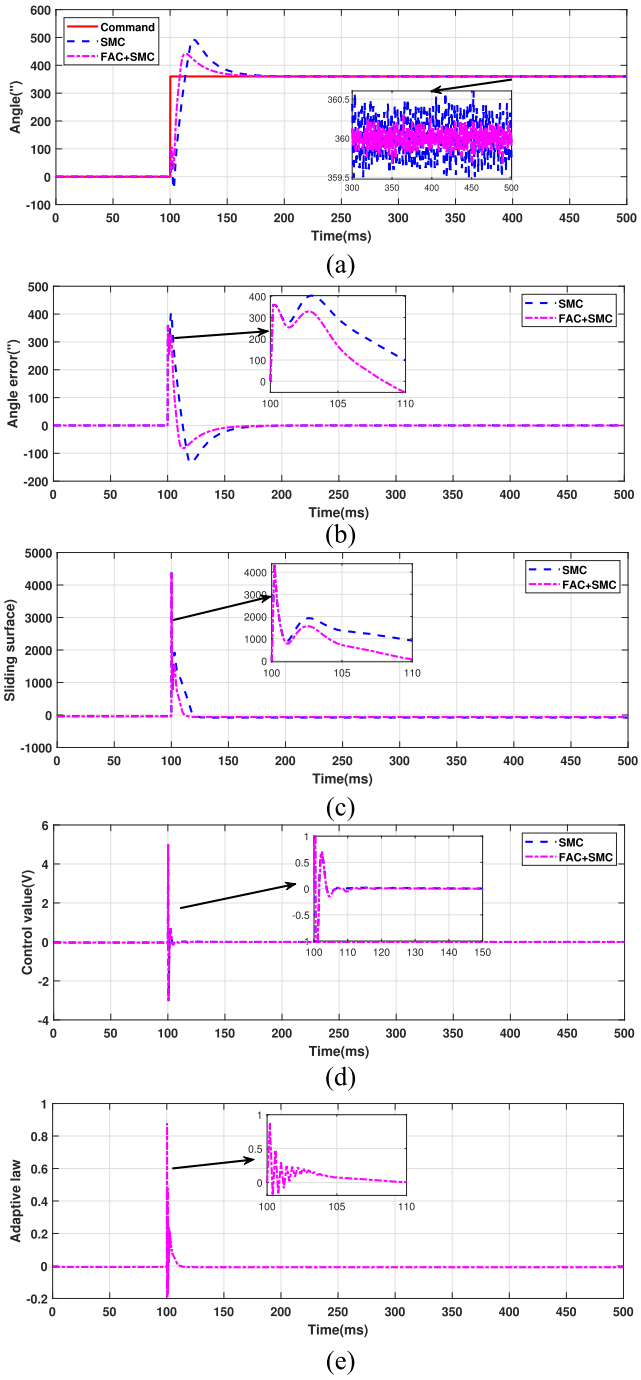

FIG. 4. Results of the step response. (a) Command and feedback signals. (b) Tracking error. (c) Sliding mode surface. (d) Control value. (e) Adaptive law.

Both methods can track the step signal, while the proposed FAC + SMC allows for a faster dynamic response and smaller steady-state error. Specifically, due to the advantages of the FAC, the rise time decreases from 13.2 to 8.4 ms, the peak time decreases from 20.4 to 13.6 ms, and the setting time decreases from 60.8 to 46.6 ms. Meanwhile, the overshoot is reduced by 38.9%. The steady-state error decreases from 1.58″ to 1.19″. The step tracking performance of FAC + SMC is better than those of SMC.

TABLE II. Performance metrics of the step response. (Boldface denotes better results.).

Metrics	SMC	FAC + SMC
Rise time (ms)	13.2	**8.4**
Peak time (ms)	20.4	**13.6**
3% setting time (ms)	60.8	**46.6**
Overshoot (%)	36.8	**22.5**
Steady-state error (″)	1.58	**1.19**

Experimental results on the rate of convergence are provided. Comparing the sliding mode surfaces of the two algorithms, the proposed FAC + SMC scheme in this investigation has a faster convergence rate than SMC. The state of the control value and the adaptive law also converges quickly after a short adjustment process, which also verifies the finite-time convergence characteristics of the proposed controller.

D. Sinusoidal signal tracking performance

To examine the tracking performance of the controller to dynamic signals, a sinusoidal signal with an amplitude of 360″ and a frequency of 10 Hz is selected as the input reference signal. The tracking response and the system states are all shown in Fig. 5.

In terms of Fig. 5, it is found that the FAC + SMC scheme generates a lower tracking error. The peak-to-peak error (PPE) of SMC is 4.51″, while that of FAC + SMC is 3.78″. The FAC + SMC and SMC lead to the root mean square error (RMSE) of 0.93″ and 1.17″, respectively. The tracking accuracy of FAC + SMC has been improved by 19.8% over the SMC method.

The control values of the two controllers are also shown in Fig. 5, and they provide smooth control actions without chattering. Moreover, we can see that the parameters are adjusted automatically during the motion tracking process, which is the reason why the proposed FAC + SMC performs better than the fixed-gain SMC. At last, the states of the system, i.e., the sliding surface s, the control value u, and the adaptive law k_a, are dynamically stable when tracking dynamic signals.

E. Robust performance against model uncertainty

To verify the robustness of the control algorithm to model uncertainty, the model parameter p_2 is selected to be artificially changed. Based on p_2 obtained in the previous model identification, we increase the uncertainty by 10% and 20%, respectively, that is, $p_2' = 1.1p_2$, $p_2'' = 1.2p_2$, where p_2' and p_2'' represent the new values for the experiments in this subsection.

The input reference is still a sinusoidal signal with a frequency of 10 Hz and an amplitude of 360″. The angle error curves of the two methods under different Δp_2 are shown in Fig. 6.

Compared to the results in Fig. 5, the angular error increases significantly with the addition of model uncertainty. However, the proposed FAC + SMC algorithm still has lower angular error than

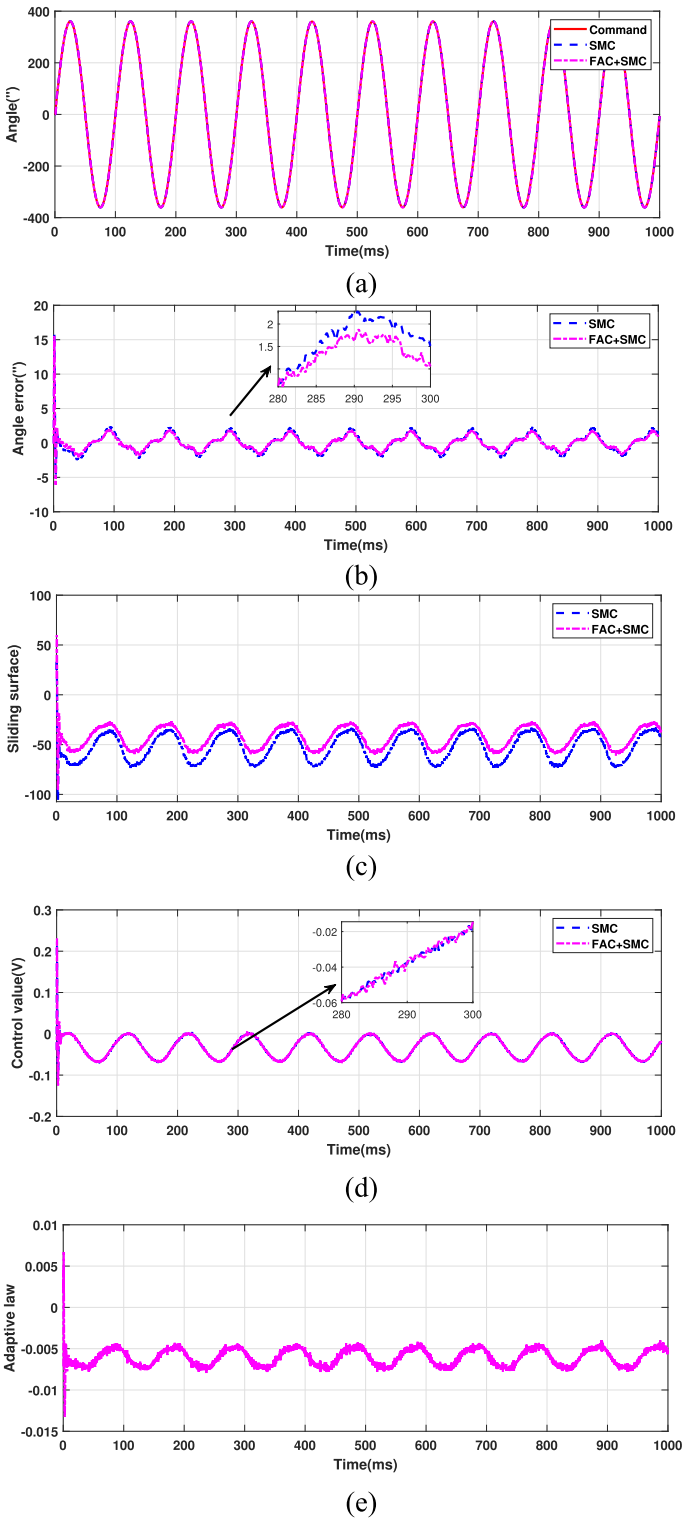

FIG. 5. Results of tracking the 10 Hz sinusoidal signal. (a) Command and feedback signals. (b) Tracking error. (c) Sliding mode surface. (d) Control value. (e) Adaptive law.

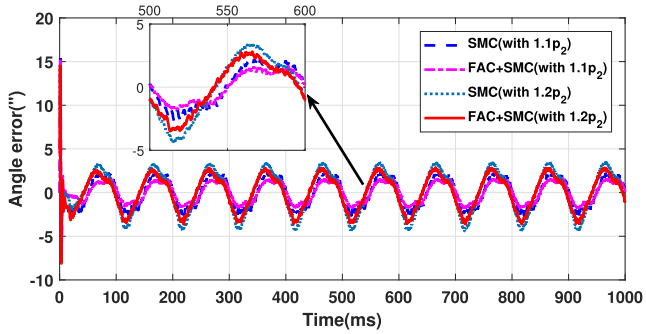

FIG. 6. Tracking results of the 10 Hz sinusoidal signal with Δp_2 variation.

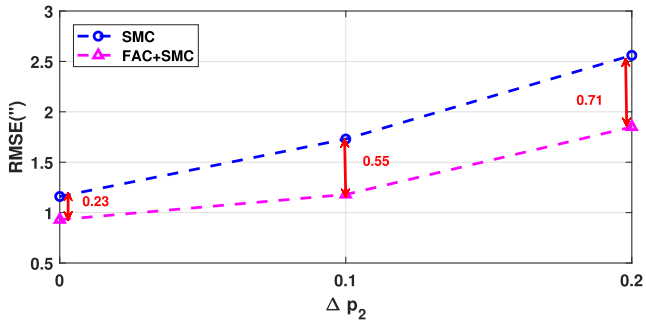

FIG. 7. RMSE of 10 Hz sinusoidal signal tracking with different Δp_2.

SMC under 10% and 20% model uncertainty. For a quantitative comparison, we present the RMSEs of the two algorithms under different model uncertainty in Fig. 7.

According to the analysis of Eq. (18), when p_2 is changed, the control value u corresponds to the addition of a time-varying disturbance. As model uncertainty increases, the RMSE increases for both methods. At 10% model uncertainty, the RMSEs for SMC and FAC + SMC are 1.73″ and 1.18″, respectively. At 20% model uncertainty, they increase to 2.56″ and 1.85″, respectively. Meanwhile, the difference between the two methods gradually increases from 0.23 to 0.55 and then to 0.71. It is suggested that the proposed FAC + SMC gradually becomes more advantageous when model uncertainty is large, and it resists the effects of model uncertainty.

V. CONCLUSION AND PROSPECT

In this paper, a robust finite-time adaptive control method based on SMC with the PID surface is proposed for a VCM-based FSM system. The finite-time convergence of the method is analyzed, and the proposed controller is implemented in DSP. The adaptive controller compensates model uncertainty while maintaining the advantages of SMC. The controller has the advantage that only one adaptive control value is added to the classical SMC, and the parameter tuning in the adaptive controller is easy, making it suitable for practical system applications. Experimental results show that the proposed method has a better step and sinusoidal signal tracking performances and robustness to model uncertainty compared with

the SMC. With the proposed controller, a high-precision motion of FSM is achieved.

The environment changes often appear in engineering applications, resulting in model changes of the controlled system. The proposed method is robust to model uncertainty and ensures a stable system with high accuracy at the same time, providing an effective reference design for engineering practice.

The proposed FAC + SMC scheme works well under model uncertainty, but the phase lag and magnitude difference problem of the FSM are obvious when the frequency of the input signal increases, so it is necessary to explore the control algorithm of the FSM under high dynamic or high bandwidth conditions in the future work.

ACKNOWLEDGMENTS

This research was supported, in part, by the National Natural Science Foundation of China under Grant No. 62103396; in part, by the China Postdoctoral Science Foundation under Grant No. 2020TQ0350; and, in part, by the Jilin Scientific and Technological Development Program under Grant No. 20200403058SF.

AUTHOR DECLARATIONS

Conflict of Interest

The authors have no conflicts to disclose.

Author Contributions

Lina Wang: Conceptualization (equal); Investigation (equal); Methodology (equal); Writing – original draft (equal). **Zhongshi Wang**: Data curation (equal); Formal analysis (equal); Writing – review & editing (equal). **Fuchao Wang**: Resources (equal); Software (equal). **Guangfeng Shi**: Validation (equal); Visualization (equal). **Rui Xu**: Funding acquisition (equal); Project administration (equal); Supervision (equal).

DATA AVAILABILITY STATEMENT

The data that support the findings of this study are available from the corresponding author upon reasonable request.

REFERENCES

[1]D. N. Van, D. D. Xuan, and D. V. Thanh, "Optical design with non-rotationally symmetric field mapping for infrared search and track system," Proc. SPIE **11895**, 118951I (2021).
[2]Y.-H. Chang, G. Hao, and C.-S. Liu, "Design and characterisation of a compact 4-degree-of-freedom fast steering mirror system based on double Porro prisms for laser beam stabilization," Sens. Actuators, A **322**, 112639 (2021).
[3]D. Lin, Y. Wu, and F. Zhu, "Research on precision tracking on fast steering mirror and control strategy," IOP Conf. Ser.: Earth Environ. Sci. **114**, 012009 (2018).
[4]C. Dribusch, M. K. Cho, J. Ryu *et al.*, "Control modeling of the fast-steering secondary mirror for GMT," Proc. SPIE **10705**, 1701–1709 (2018).
[5]Y. Fan, Y. He, and U.-X. Tan, "Real-time compensation system via gyroscope and fast steering mirror for wide-bandwidth multiple-frequency vehicle disturbance," IEEE ASME Trans. Mechatron. **25**(2), 650–660 (2020).
[6]M. K. Masten, "Inertially stabilized platforms for optical imaging systems: Tracking dynamic targets with mobile sensors," IEEE Control Syst. Mag. **28**(1), 47–64 (2008).
[7]D. J. Kluk, M. T. Boulet, and D. L. Trumper, "A high-bandwidth, high-precision, two-axis steering mirror with moving iron actuator," Mechatronics **22**(3), 257–270 (2012).
[8]W. W. Han, S. B. Shao, S. W. Zhang *et al.*, "Design and modeling of decoupled miniature fast steering mirror with ultrahigh precision," Mech. Syst. Signal Process. **167**, 108521 (2022).
[9]J. Zhong, L. Li, R. Nishida *et al.*, "Design and evaluation of a PEA-driven fast steering mirror with a permanent magnet preload force mechanism," Precis. Eng. **62**, 95–105 (2020).
[10]Z. S. Wang, R. Xu, L. N. Wang *et al.*, "Finite-time adaptive sliding mode control for high-precision tracking of piezo-actuated stages," ISA Trans. **129**, 436–445 (2021).
[11]Z. Gong, D. H. Huo, Z. Y. Niu *et al.*, "A novel long-stroke fast tool servo system with counterbalance and its application to the ultra-precision machining of microstructured surfaces," Mech. Syst. Signal Process. **173**, 109063 (2022).
[12]A. Al-Jodah, B. Shirinzadeh, M. Ghafarian *et al.*, "A fuzzy disturbance observer based control approach for a novel 1-DOF micropositioning mechanism," Mechatronics **65**, 102317 (2020).
[13]Z. Gong, D. Huo, Z. Niu *et al.*, "Investigation of control algorithm for long-stroke fast tool servo system," Precis. Eng. **75**, 12–23 (2022).
[14]R. Wang, X. Yin, Q. Wang *et al.*, "Direct amplitude control for voice coil motor on high frequency reciprocating rig," IEEE ASME Trans. Mechatron. **25**(3), 1299–1309 (2020).
[15]A. Bekkali, H. Fujita, and M. Hattori, "New generation free-space optical communication systems with advanced optical beam stabilizer," J. Light Technol. **40**(5), 1509–1518 (2022).
[16]K. D. Wang, X. Q. Su, Z. Li, and S. B. Wu, "ADRC system of FSM for image motion compensation," Proc. SPIE **10256**, 1025604 (2017).
[17]Z. Wang, B. Zhang, X. Li, and S. Zhang, "Study on application of model reference adaptive control in fast steering mirror system," Optik **172**(9), 995–1002 (2018).
[18]Z. Ning, Y. Mao, Y. Huang *et al.*, "Robust current control of voice coil motor in tip-tilt mirror based on disturbance observer framework," IEEE Access **9**, 96814–96822 (2021).
[19]T. Tang, S. Xu Niu, T. Yang *et al.*, "Vibration rejection of Tip-Tilt mirror using improved repetitive control," Mech. Syst. Signal Process. **116**, 432–442 (2019).
[20]A. Polyakov and L. Fridman, "Stability notions and lyapunov functions for sliding mode control systems," J. Franklin Inst. **351**(4), 1831–1865 (2014).
[21]S. Kuang, X. K. Guan, and D. Y. Dong, "Finite-time stabilization control of quantum systems," Automatica **123**, 109327 (2021).
[22]X. Wang, G. Wang, and S. Li, "Distributed finite-time optimization for disturbed second-order multiagent systems," IEEE Trans. Cybern. **51**(9), 4634–4647 (2021).
[23]Y. Shtessel, L. Fridman, and F. Plestan, "Adaptive sliding mode control and observation," Int. J. Control **123**, 1743 (2016).
[24]J. Wu and R.-r. Ma, "Robust finite-time and fixed-time chaos synchronization of PMSMs in noise environment," ISA Trans. **119**, 65–73 (2022).
[25]N. Wang, H. R. Karimi, H. Li *et al.*, "Accurate trajectory tracking of disturbed surface vehicles: A finite-time control approach," IEEE ASME Trans. Mechatron. **24**(3), 1064–1074 (2019).
[26]E. Moulay, V. Léchappé, E. Bernuau *et al.*, "Robust fixed-time stability: Application to sliding-mode control," IEEE Trans. Autom. Control **67**(2), 1061–1066 (2022).
[27]S. P. Bhat and D. S. Bernstein, "Finite-time stability of continuous autonomous system," SIAM J. Control Optim. **38**(3), 751–766 (2000).
[28]Y. Shen and X. Xia, "Semi-global finite-time observers for nonlinear systems," Automatica **44**(12), 3152–3156 (2008).